Supplemental Figures

Adaptation of centromere to breakage through local genomic and epigenomic remodeling in wheat

Jingwei Zhou[#], Yuhong Huang[#], Huan Ma, Yiqian Chen, Chuanye Chen, Fangpu Han, Handong Su[*]

Table of Contents

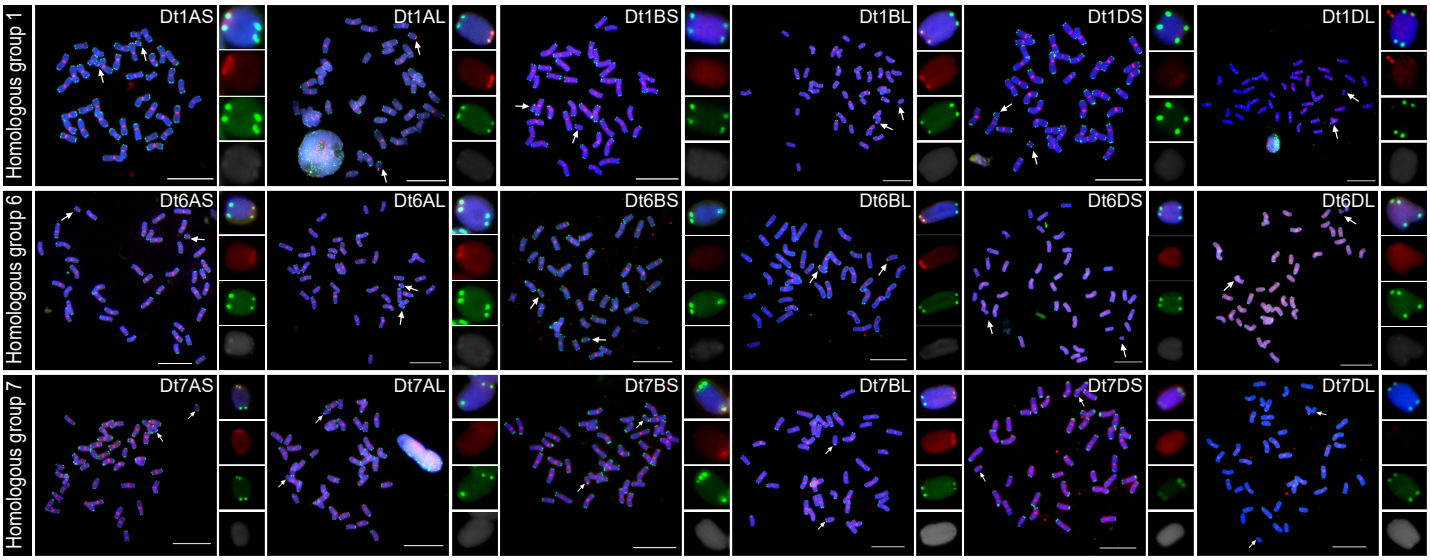

Supplemental Fig. S1. Detection of centromere and telomere signals on mitotic chromosomes in wheat ditelosomic stocks from homoeologous groups 1, 6 and 7. Fluorescence *in situ* hybridization (FISH) was performed to visualize the distribution of centromeric and telomeric signals on mitotic chromosomes of wheat ditelosomic lines corresponding to homoeologous groups 1 (top panels), 6 (middle) and 7 (bottom). Root tip metaphase spreads were prepared for each line. Arrows highlight the telocentric chromosomes in each panel on the right provide high-magnification views of the identified ditelosomic chromosomes to better resolve centromere and telomere signals. The observed signal patterns confirm the expected chromosomal structure in the ditelosomic lines. Centromeres were labeled using CRW probe (red fluorescence), while telomere were detected with a telomere-specific probe (green fluorescence). Chromosomes were counterstained blue with 4',6-Diamidino-2-phenylindole (DAPI), allowing clear visualization of chromosomal morphology. The scale bar is 20 µm.

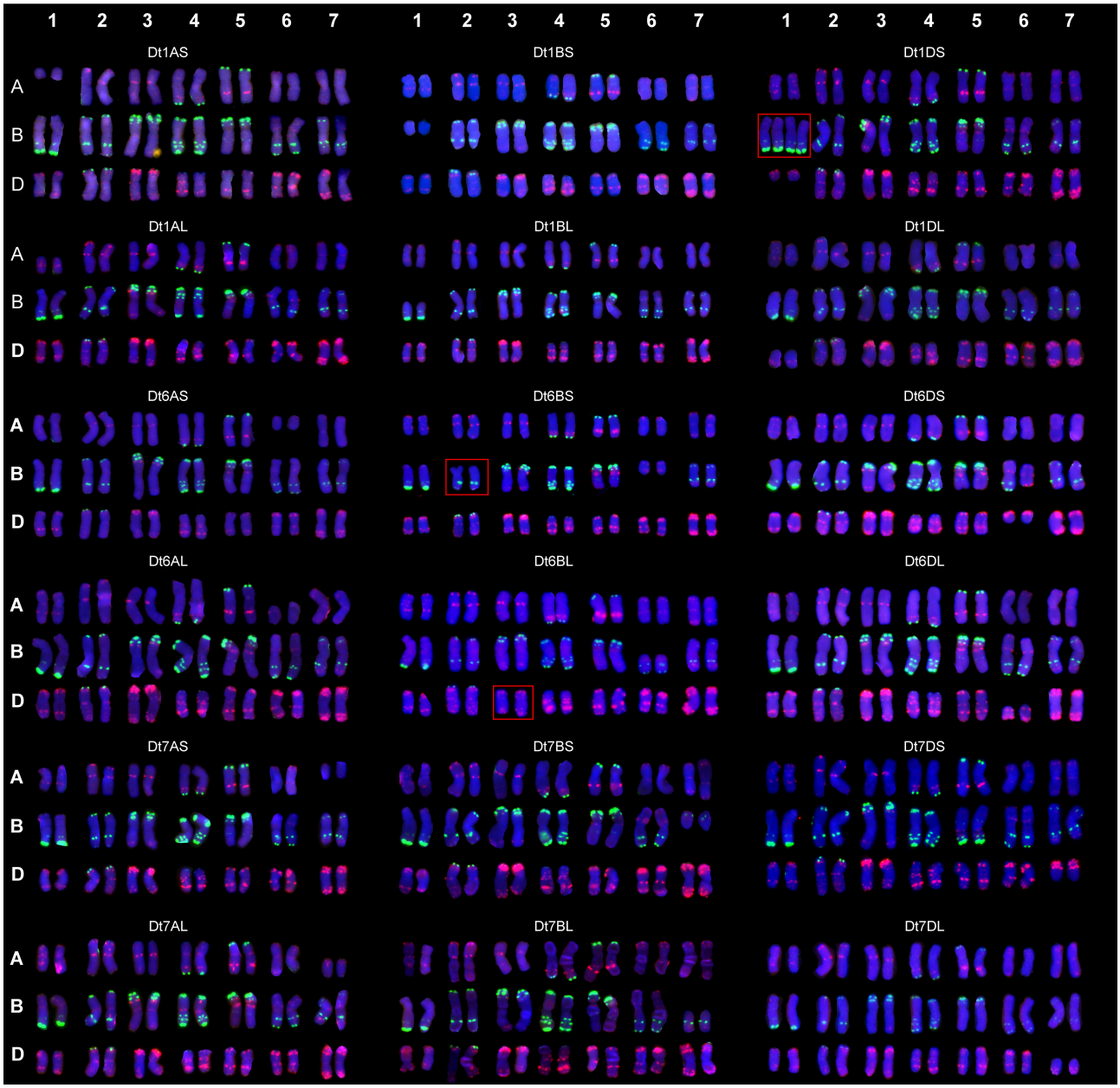

Supplemental Fig. S2. Karyotype analysis reveals chromosomal structural variations in wheat ditelosomic lines from homoeologous groups 1, 6, and 7. Metaphase chromosome spreads from root tips of wheat ditelosomic stocks corresponding to homoeologous groups 1, 6, and 7 were analyzed using FISH to detect chromosomal structural and numerical variations. Two repetitive sequence probes were used for karyotyping. pTa535-1 (red) and pSc119.2-1 (green) predominantly labels specific chromosomal regions and highlights terminal and interstitial sites on certain chromosomes. Red boxes highlight chromosomes exhibiting structural rearrangements (e.g., deletions, or duplications) or copy number variations that are specific to individual ditelosomic lines. Chromosomes were counterstained with DAPI (blue) to visualize overall morphology. These karyotype assays provide supporting cytological evidence for some chromosomal alterations in the wheat ditelosomic stocks analyzed.

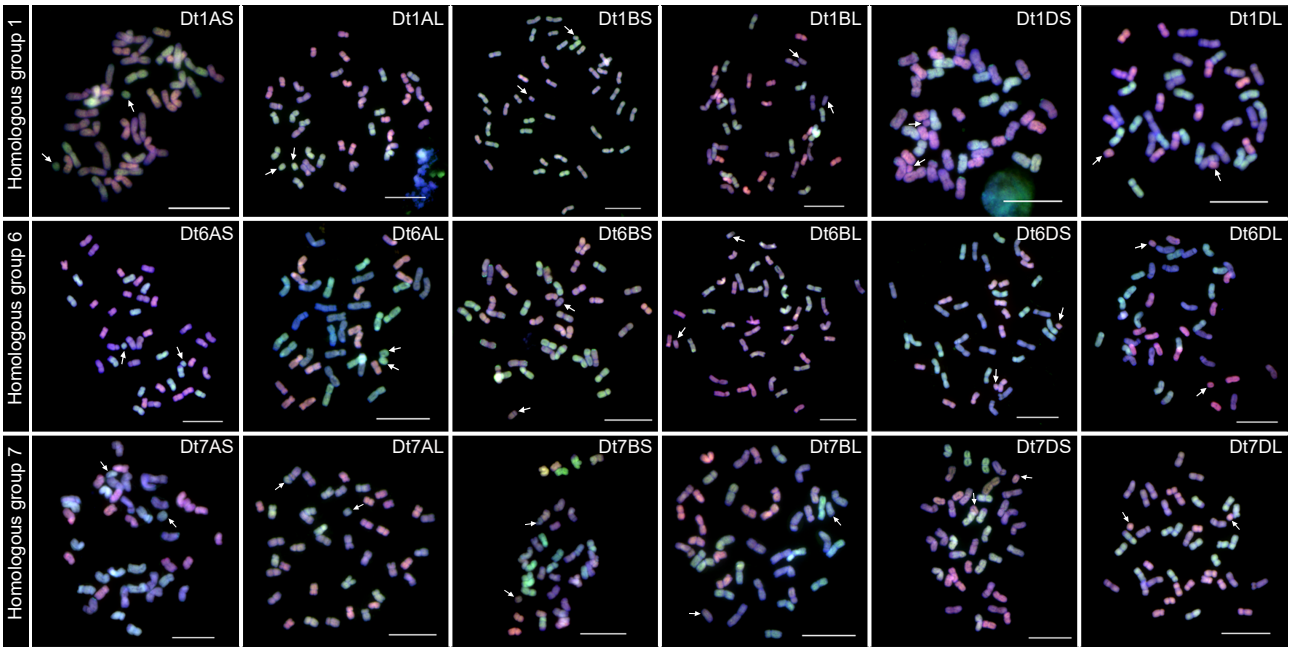

Supplemental Fig. S3. Cytological detection of homoeologous recombination in wheat ditelosomic lines of homoeologous groups 1, 6 and 7. Multi-color FISH analyses was performed on metaphase chromosome spreads from root tips of wheat ditelosomic stocks derived from homoeologous groups 1 (top panels), 6 (middle) and 7 (bottom) to examine homoeologous recombination and chromosomal segment origins. Genomic DNA from *Aegilops tauschii* was labeled in red, *Triticum urartu* in green, and *Ae. speltoides* genomic DNA was used as a blocking agent, minimizing non-specific hybridization from the B-genome background. White arrows indicate the telocentric chromosomes in each panel, where no potential homoeologous exchanges and introgression events between subgenome segments can be observed in the ditelosomic chromosomes. The scale bar is 20 μm.

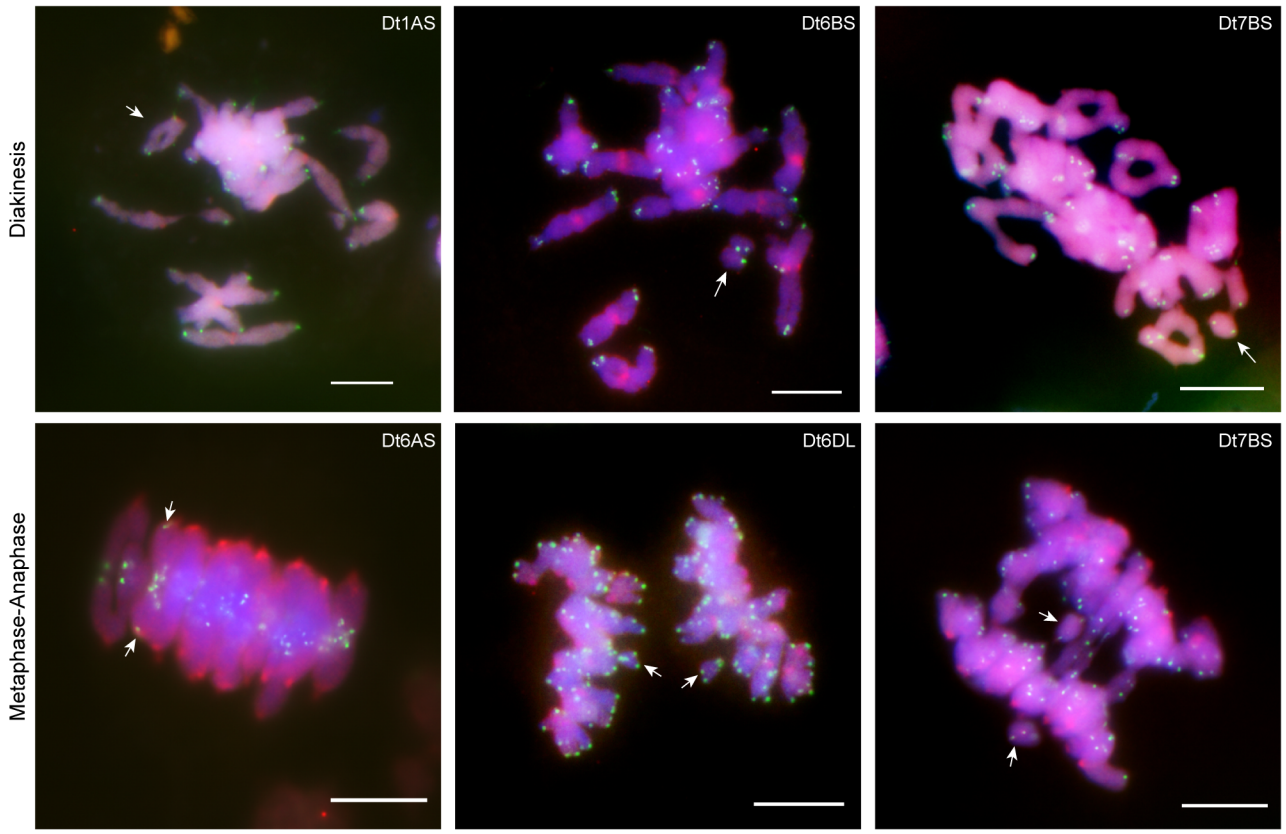

Supplemental Fig. S4. Observation of meiotic chromosome behavior in wheat ditelosomic lines. FISH was used to examine the behavior of telocentric chromosomes during meiosis in wheat ditelosomic stocks. Diakinesis (top panels) and Metaphase I to Anaphase I transition (bottom panels) were shown. Arrows indicate telocentric chromosomes. Centromeres were labeled with the CRW probe (red fluorescence), and telomeres were detected using a telomere-specific probe (green fluorescence). White arrows indicate telocentric chromosomes with proper centromere-telomere labeling and support cytological analysis of meiotic behavior in structurally altered centromeres. Chromosomes were counterstained with DAPI (blue), allowing visualization of overall chromatin structure. The scale bar is 20 μm.

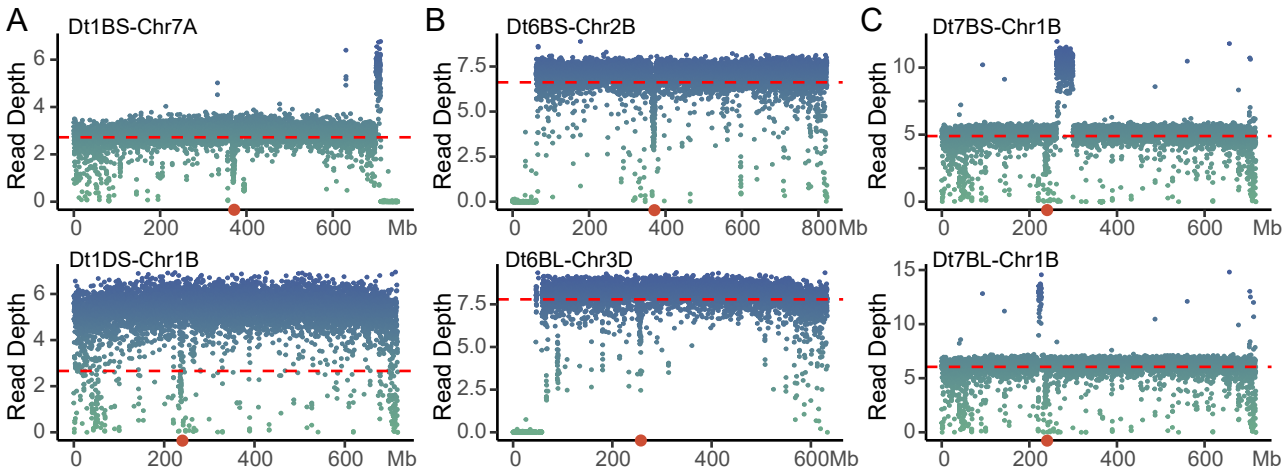

Supplemental Fig. S5. Detection of chromosomal structural variations based on sequencing depth analysis in wheat ditelosomic lines. (A) Examples of copy number variations (CNVs) identified at the terminal or chromosomal levels in specific lines. In Dt1BS, a segmental duplication and adjacent deletion are detected at the terminal regions of chromosome 7A. In Dt1DS, a complete whole- chromosome duplication of chromosome 1B is observed. (B) Detection of large deletion events in other ditelosomic lines including a 61.1-Mb terminal deletion on chromosome 2B in Dt6BS, and two deletions at the terminals of chromosome 3D in Dt6BL, measuring 46.0-Mb and 6.59-Mb, respectively. (C) Representative interstitial duplications identified within chromosome 1B, including a 37.7-Mb internal duplication in the Dt7BS line, and a 7.2-Mb duplication in Dt7BL line. For panels B-D, read depth values were calculated in 100-kb non-overlapping windows and normalized for cross-sample comparisons. The coverage lines represent sequencing depth, and red dots mark the approximate positions of centromeres.

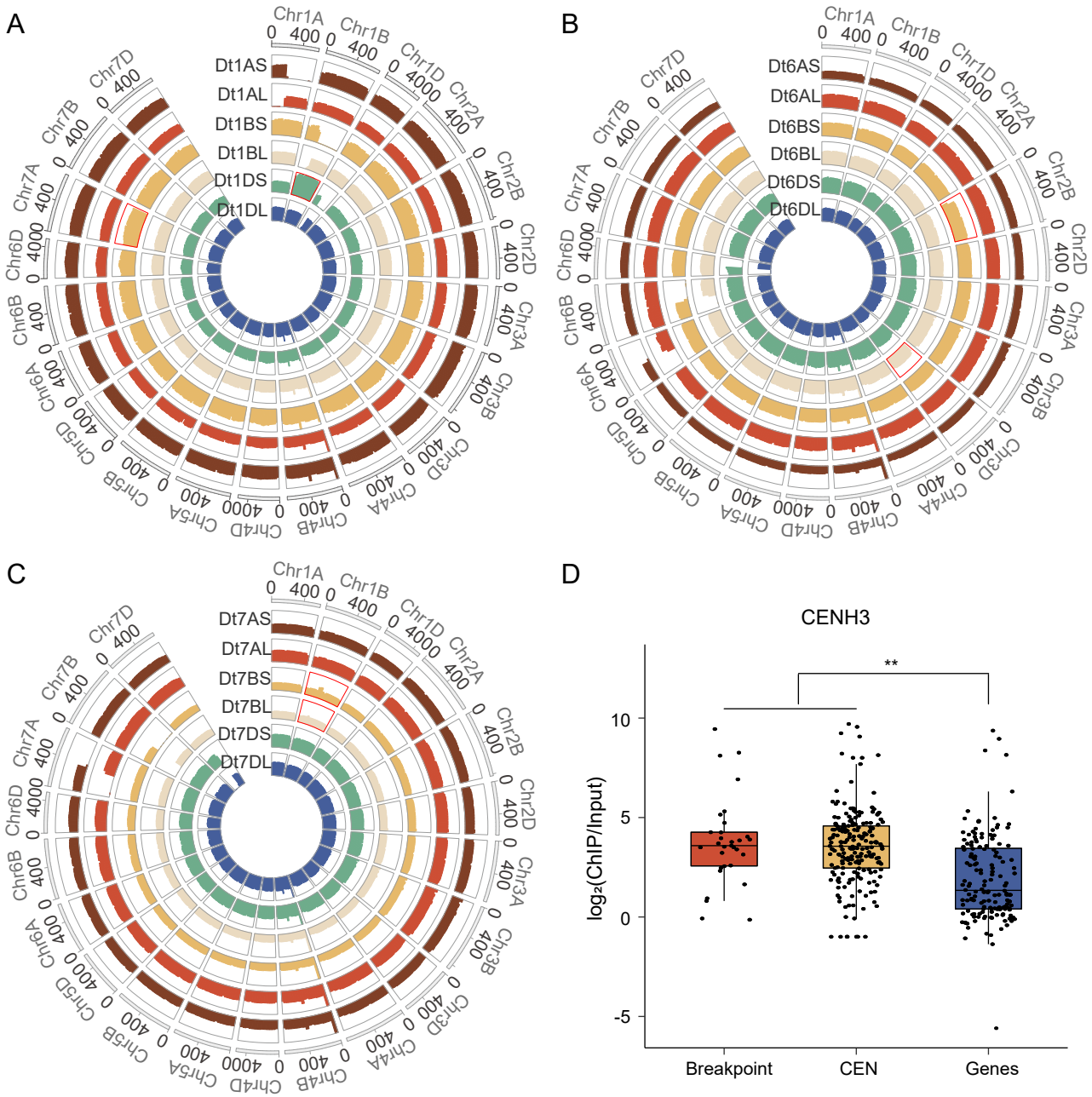

Supplemental Fig. S6. Genome-wide sequencing depth analysis identifying putative centromere breakpoint-associated regions and their CENH3 enrichments in wheat ditelosomic lines. (A-C) Circos plots visualize normalized whole-genome sequencing (WGS) read depth distributions across wheat chromosomes in ditelosomic lines from homoeologous groups 1 (left), 6 (center), and 7 (right). Each concentric track represents a different ditelosomic line, with sequencing depth in 20-Mb windows. Red rectangles indicate chromosomal regions exhibiting structural variations, such as deletions or duplications. (D) Relative enrichment levels of CENH3 (log_2(ChIP/Input)) are quantified around putative centromere breakpoint-associated regions (Breakpoint), centromeric regions (CEN), and genes located within centromeres (Genes) in CS wheat. Statistical significance is determined using Student's *t*-test, with ** $P < 0.01$.

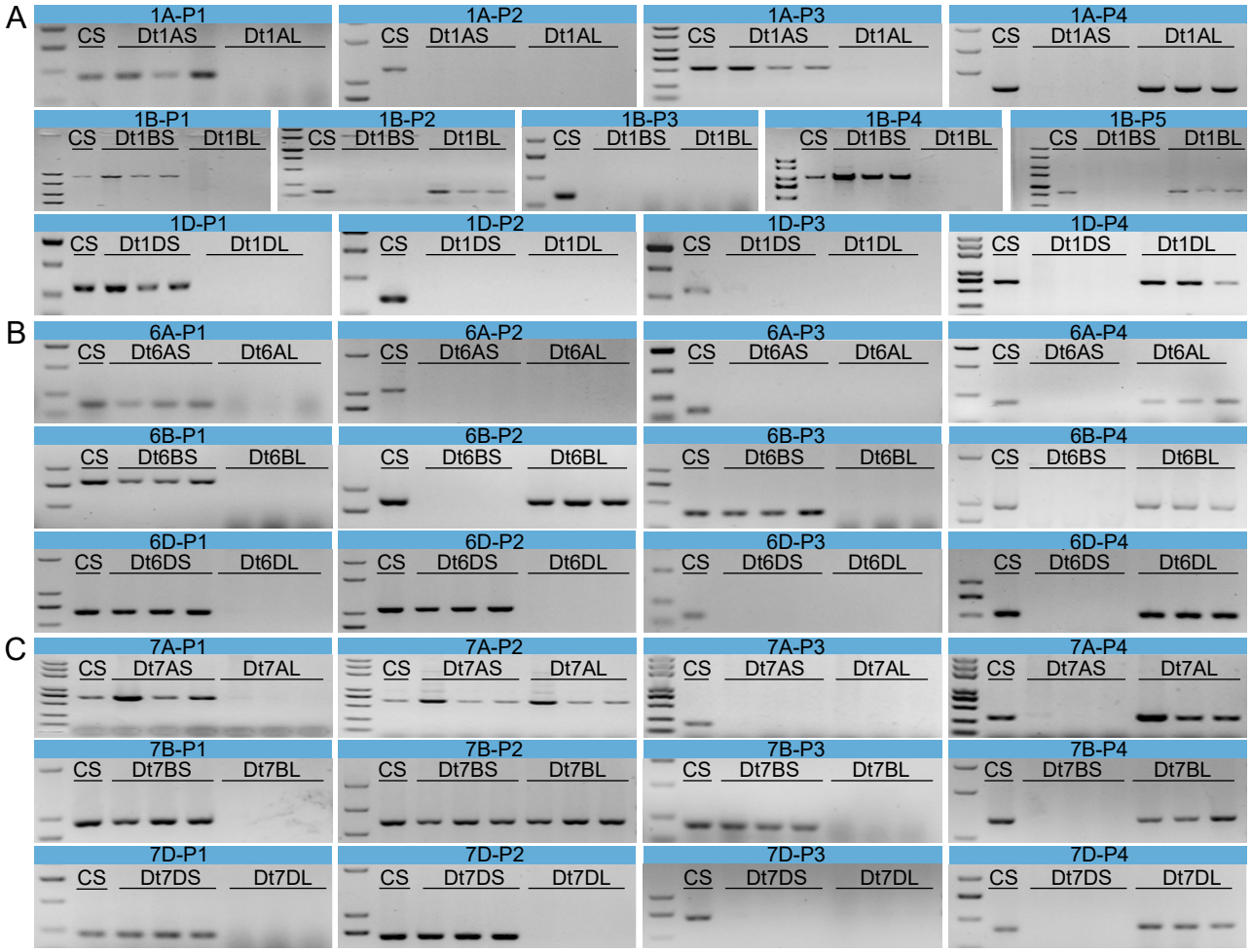

Supplemental Fig. S7. PCR validation of chromosome fragment presence or deletion in wheat ditelosomic lines compared to CS wheat. PCR assays were performed to validate the presence or absence of specific chromosomal fragments located near centromeric regions in ditelosomic lines from homoeologous groups 1 (A), 6 (B), and 7 (C). Genomic DNA was extracted from Chinese Spring (CS) wheat and corresponding short- and long-arm telosomes of each ditelosomic stock. Primer pairs targeting conserved loci flanking structurally variable centromeric regions were designed and used for amplification. The names of each primer set (e.g., 1A-P1 to 1A-P4, 6D-P1 to 6D-P4, etc.) are labeled above the corresponding lanes. Each agarose gel panel displays amplification results for specific homoeologous chromosomes. Green horizontal bars in the agarose gel electrophoresis images indicate successful amplification, confirming fragment presence, while missing bands denote deletion of the corresponding genomic region in the tested line. These PCR-based verifications support the conclusions drawn from sequencing-based structural variation analyses and confirm centromere-proximal rearrangements in the ditelosomic lines.

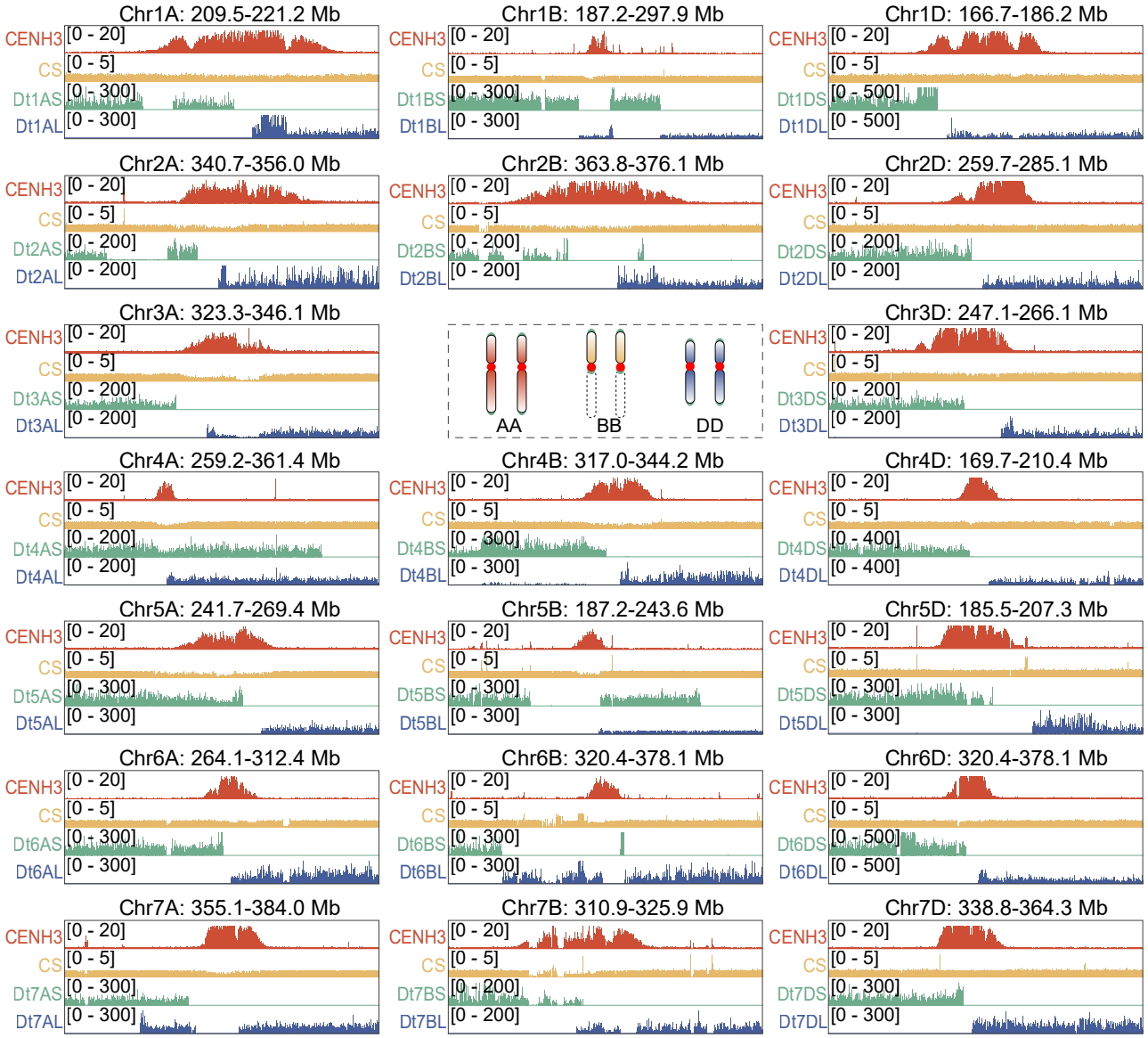

Supplemental Fig. S8. Detection of chromosomal structural variations using publicly available whole-genome resequencing data of wheat ditelosomic lines. This figure presents a genome-wide analysis of structural variations near centromeric regions in wheat ditelosomic stocks, using public resequencing datasets. Tracks illustrate the normalized genomic read depth in 10-bp bins across chromosomes from seven wheat homoeologous groups (1 to 7). For each chromosome, four layers are displayed. The top track shows the CENH3 ChIP-seq signal defining centromeric domains in Chinese Spring (CS) wheat. The subsequent three tracks display DNA resequencing coverage from CS wheat and the corresponding short-arm (S) and long-arm (L) telosomes from ditelosomic lines. These comparative depth profiles allow detection of structural variations, such as segmental deletions, duplications, or altered coverage surrounding centromere breakpoints. Notably, chromosome 3B, the largest chromosome in wheat genome, lacks ditelosomic resequencing data and is therefore excluded from this comparative analysis. Read depths are normalized using Reads Per Genomic Content (RPGC) to ensure comparability across samples.

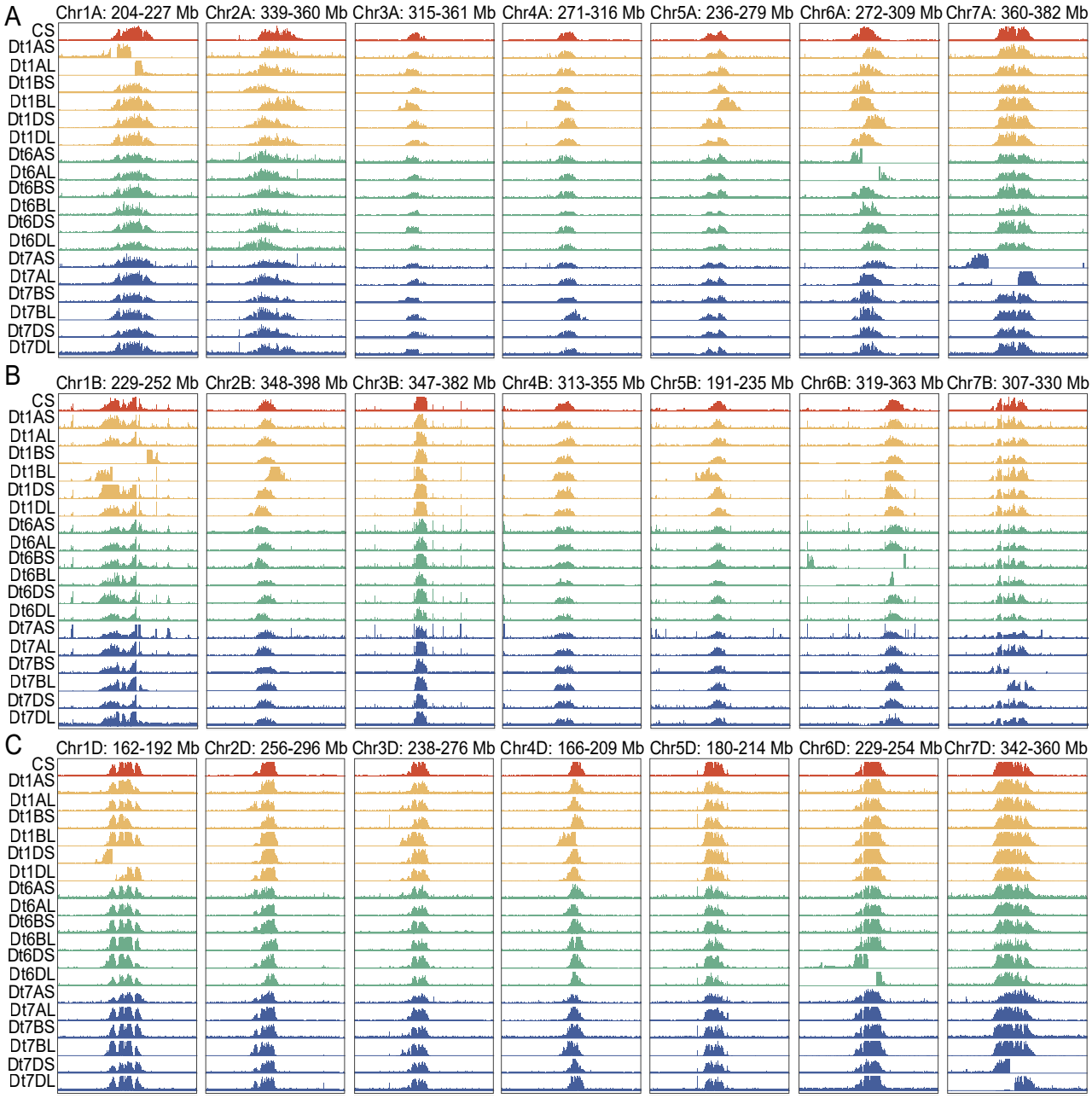

Supplemental Fig. S9. Comparative analysis of functional centromere positioning across wheat ditelosomic lines and CS reference chromosome. This figure illustrates the distribution and positional variation of CENH3-enriched functional centromeres across the AA (panel A), BB (panel B), and DD (panel C) subgenomes in wheat. CENH3 ChIP-seq signal tracks are shown for CS wheat and all ditelosomic lines from homoeologous groups 1, 6, and 7. Each line is represented by two telocentric chromosomes (short-armed and long-armed), allowing detailed comparison of centromeric localization under conditions of structural change. In each panel, the horizontal axis represents individual chromosomes (e.g., Chr1A–Chr7A for the A subgenome), with the x-axis coordinates corresponding to chromosome length in megabases (Mb). The vertical axis shows the tracks represent CENH3 ChIP-seq signal intensity. Color coding distinguishes different sources: CS wheat is represented in red, group 1 ditelosomics in orange, group 6 in green, and group 7 in blue. Shifts or disruptions in CENH3 signal positions indicate neocentromere formation, centromere repositioning, or partial centromere retention in response to chromosome breakage. This cross-subgenomic comparison highlights both conserved and variable centromere behaviors among the ditelosomic lines and provides understanding for centromere remodeling dynamics following chromosomal misdivision or rearrangement.

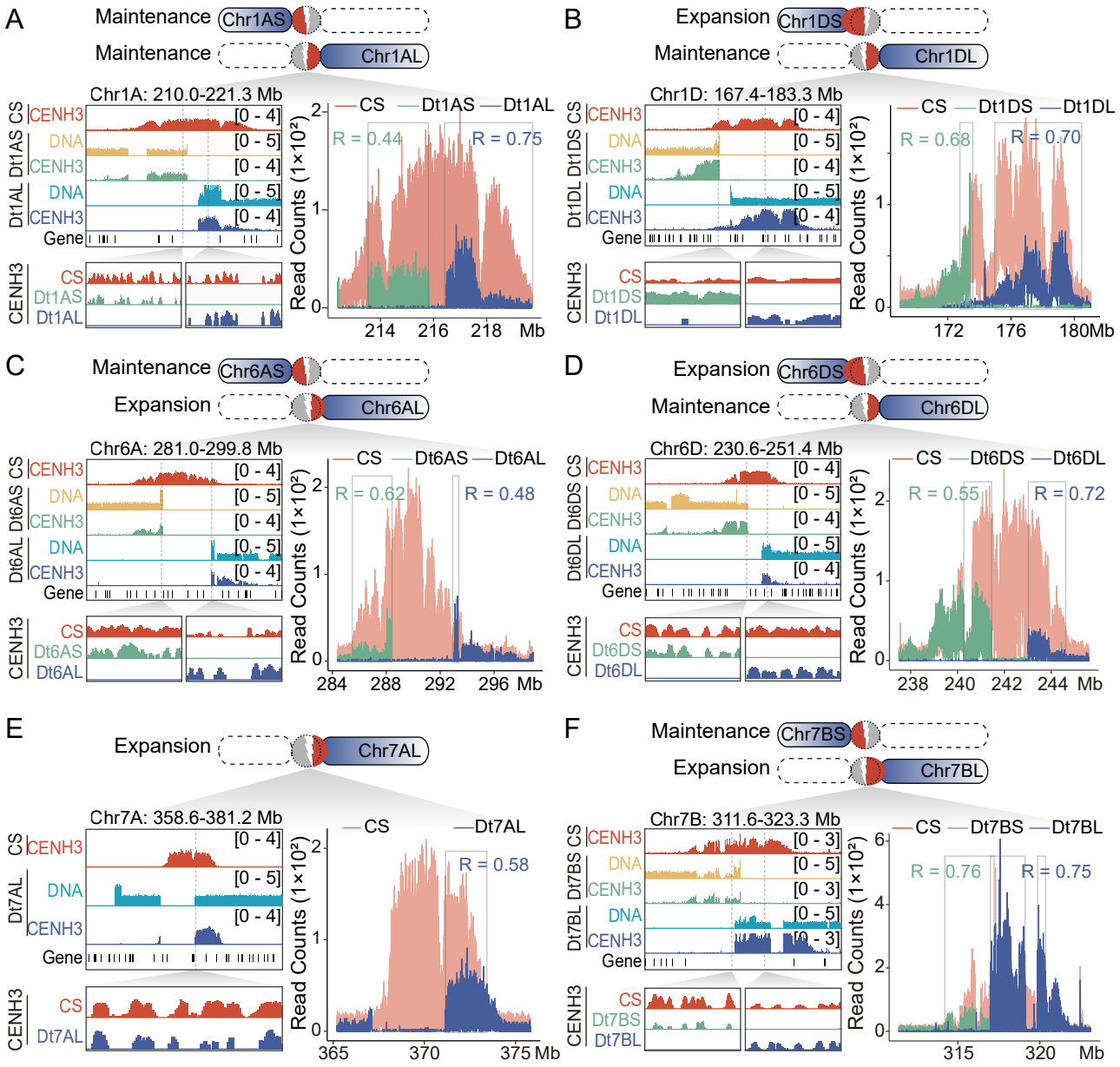

Supplemental Fig. S10. Centromere structural dynamics in wheat ditelosomic lines compared with their corresponding chromosomes in CS wheat. (A-F) Comparative analysis of centromere architecture was conducted between ditelosomic lines and their corresponding chromosomes in CS wheat across homoeologous groups 1, 6, and 7. Each panel displays the distribution of CENH3-enriched nucleosome (as detected by ChIP-seq) over a representative centromeric interval, visualized through IGV snapshots. Read coverage is shown as $\log_2$(ChIP/Input) values, aligned with gene annotations and centromere positions. Panels A-C: centromere structures in lines Dt1AS, Dt1AL, Dt1DL, Dt6AS, Dt6DL and Dt7BS show a high degree of structural conservation, with centromere boundaries and CENH3 localization largely maintained compared to CS wheat. Panels D-F: in contrast, centromere expansion is observed in lines Dt1DS, Dt6AL, Dt6DS, Dt7AL, and Dt7BL, evidenced by broader CENH3 distribution domains and additional flanking signal peaks. To quantify centromere remodeling, Pearson correlation coefficients (R values) were calculated based on CENH3 enrichment patterns within shared centromere intervals between each ditelosomic chromosome and its CS counterpart. R values are displayed within each IGV snapshot, indicating degrees of structural conservation or divergence. This analysis highlights the diversity of centromeric responses following misdivision, ranging from complete maintenance to substantial expansion, underscoring the dynamic and plastic nature of centromere architecture in wheat.

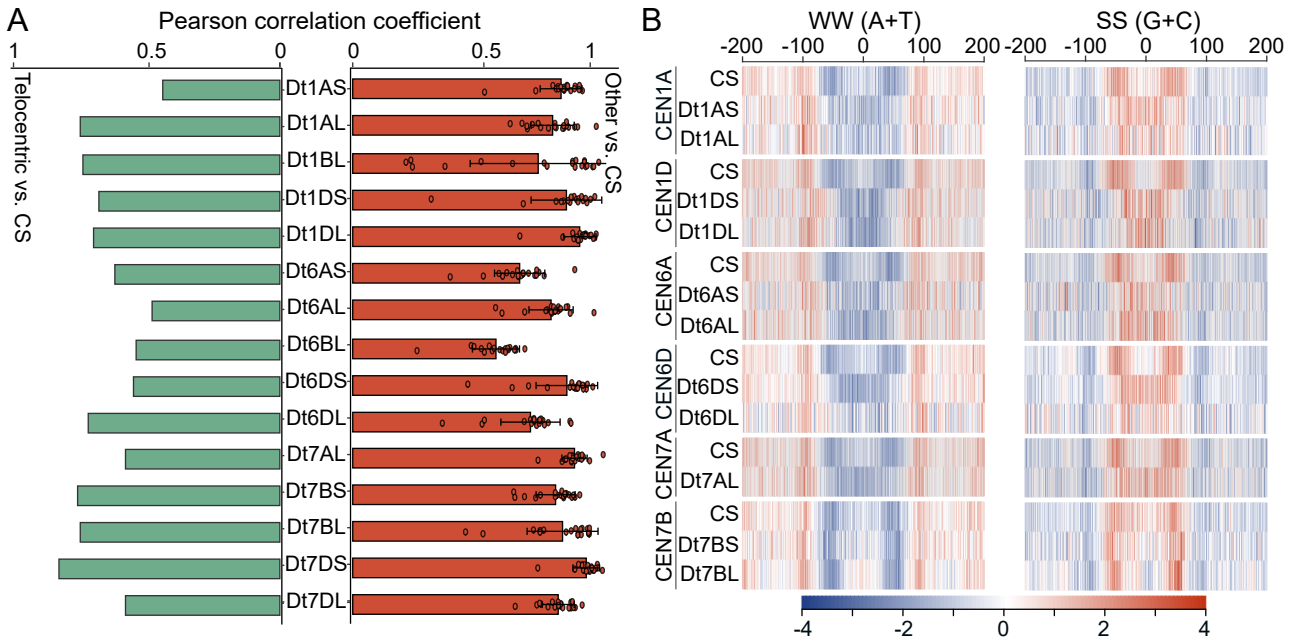

Supplemental Fig. S10. Centromere structural dynamics in wheat ditelosomic lines compared with their corresponding chromosomes in CS wheat. (A-F) Comparative analysis of centromere architecture was conducted between ditelosomic lines and their corresponding chromosomes in CS wheat across homoeologous groups 1, 6, and 7. Each panel displays the distribution of CENH3-enriched nucleosome (as detected by ChIP-seq) over a representative centromeric interval, visualized through IGV snapshots. Read coverage is shown as $\log_2$(ChIP/Input) values, aligned with gene annotations and centromere positions. Panels A-C: centromere structures in lines Dt1AS, Dt1AL, Dt1DL, Dt6AS, Dt6DL and Dt7BS show a high degree of structural conservation, with centromere boundaries and CENH3 localization largely maintained compared to CS wheat. Panels D-F: in contrast, centromere expansion is observed in lines Dt1DS, Dt6AL, Dt6DS, Dt7AL, and Dt7BL, evidenced by broader CENH3 distribution domains and additional flanking signal peaks. To quantify centromere remodeling, Pearson correlation coefficients (R values) were calculated based on CENH3 enrichment patterns within shared centromere intervals between each ditelosomic chromosome and its CS counterpart. R values are displayed within each IGV snapshot, indicating degrees of structural conservation or divergence. This analysis highlights the diversity of centromeric responses following misdivision, ranging from complete maintenance to substantial expansion, underscoring the dynamic and plastic nature of centromere architecture in wheat.

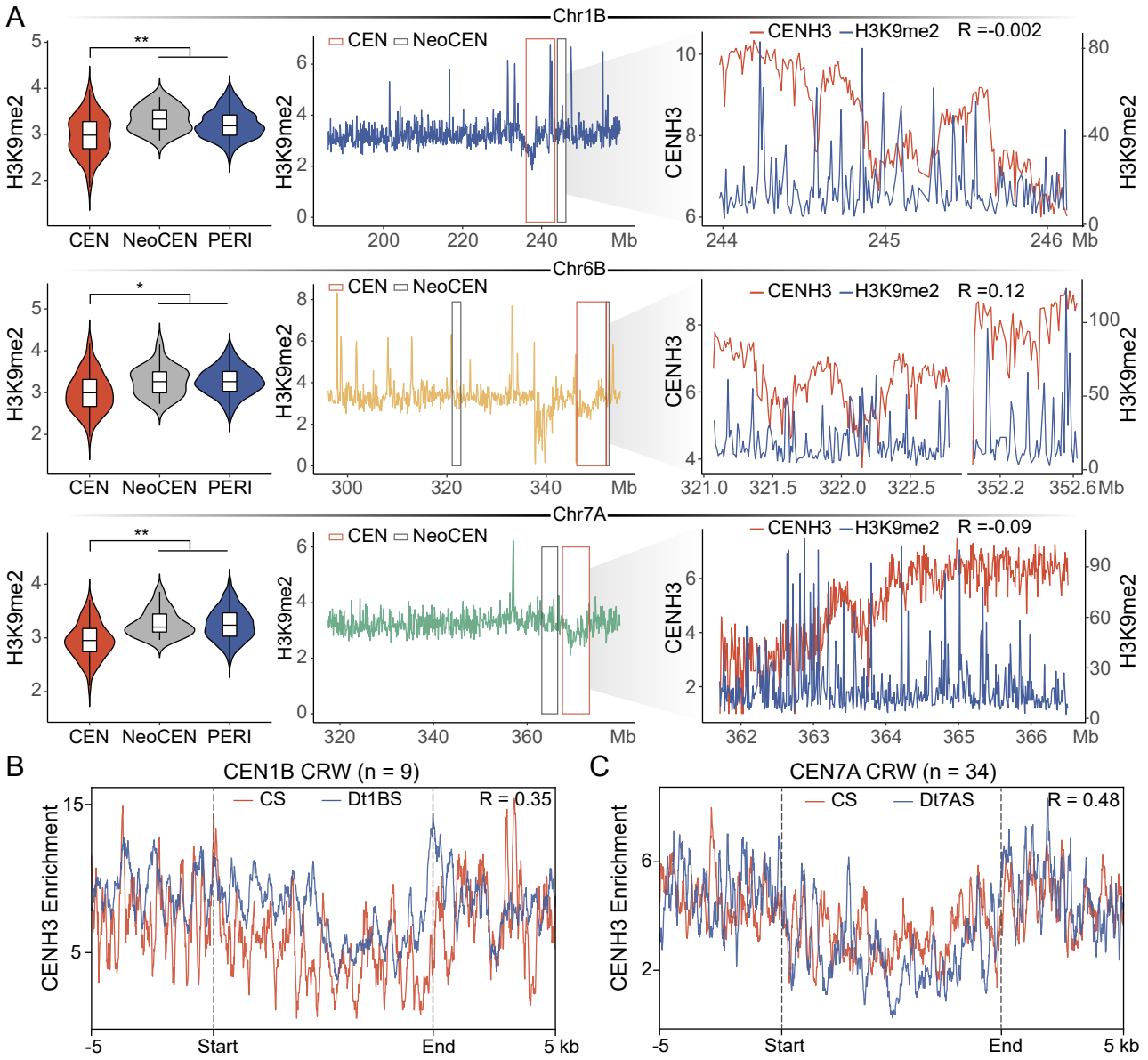

Supplemental Fig. S12. Epigenetic and sequence features associated with neocentromere formation in wheat ditelosomic lines. (A) Comparative analysis of heterochromatin states across three genomic regions — native centromeres (CEN), neocentromeres (NeoCEN) and flanking pericentromeric (PERI) regions in ditelosomic lines Dt1BS, Dt6BS, and Dt7AS. ChIP-seq profiling of the repressive histone modification H3K9me2 in CS wheat is used to assess the chromatin landscape prior to neocentromere establishment. H3K9me2 signal intensities were averaged across 10-kb bins spanning each region. Enlarged IGV views highlight the inverse correlation (or lack thereof) between CENH3 enrichment (red) and H3K9me2 levels (blue), providing insight into the chromatin context conducive to neocentromere formation. Correlation coefficients (R values) between CENH3 and H3K9me2 distributions are shown for each locus. Statistical significance is determined using Student's *t*-test, with * $P < 0.05$; ** $P < 0.01$. (B-C) Analysis of CENH3 nucleosome distribution relative to CRW centromeric repeats in neocentromeric regions of Dt1BS (B) and Dt7AS (C) compared to their corresponding CS chromosomes. Metaprofiles illustrate the average CENH3 enrichment ±5 kb surrounding CRW repeat arrays. The red curve represents CS wheat; the blue curve corresponds to the ditelosomic line. Pearson correlation coefficients (R values) reflect the degree of alignment between CENH3 binding patterns and CRW sequence positioning. Notably, no complete CRW repeat units were identified within the neocentromeric region of Dt6BS. These results suggest that neocentromeres can arise in regions depleted of canonical centromeric repeats but with locally altered chromatin states, underscoring the epigenetically plastic nature of centromere specification.

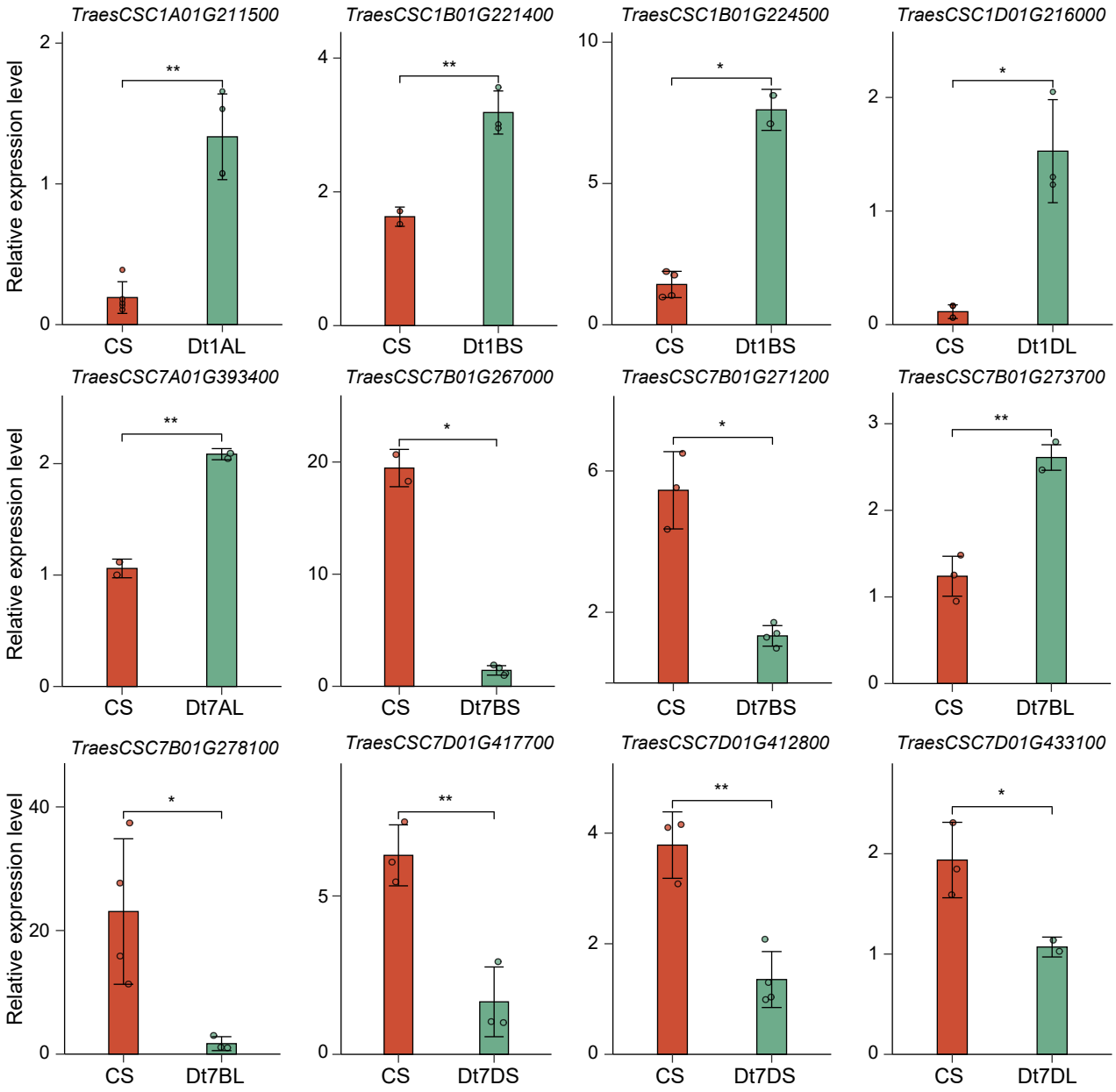

Supplemental Fig. S13. RT-PCR validation of differentially expressed genes (DEGs) in centromeric and pericentromeric regions of wheat ditelosomic lines. A subset of significant differentially expressed genes (DEGs), identified through RNA-seq analysis within centromeric and pericentromeric regions, were randomly selected for independent validation via RT-PCR. Gene expression levels were compared between CS and various ditelosomic wheat lines, including Dt1AL, Dt1BS, Dt1DL, Dt7AL, Dt7BL, Dt7BS, Dt7DL, and Dt7DS. The tested genes include loci from subgenomes A, B, and D, and their expression levels are shown as relative fold change. Each bar represents the mean ± standard deviation of at least three biological replicates. Asterisks indicate statistical significance based on Student's *t*-test (* $P < 0.05$; ** $P < 0.01$). Primer sequences and amplification details are listed in Supplemental Table S2. This analysis confirms the reliability of RNA-seq–based DEG identification and highlights altered gene expression patterns associated with centromere remodeling in ditelosomic lines.

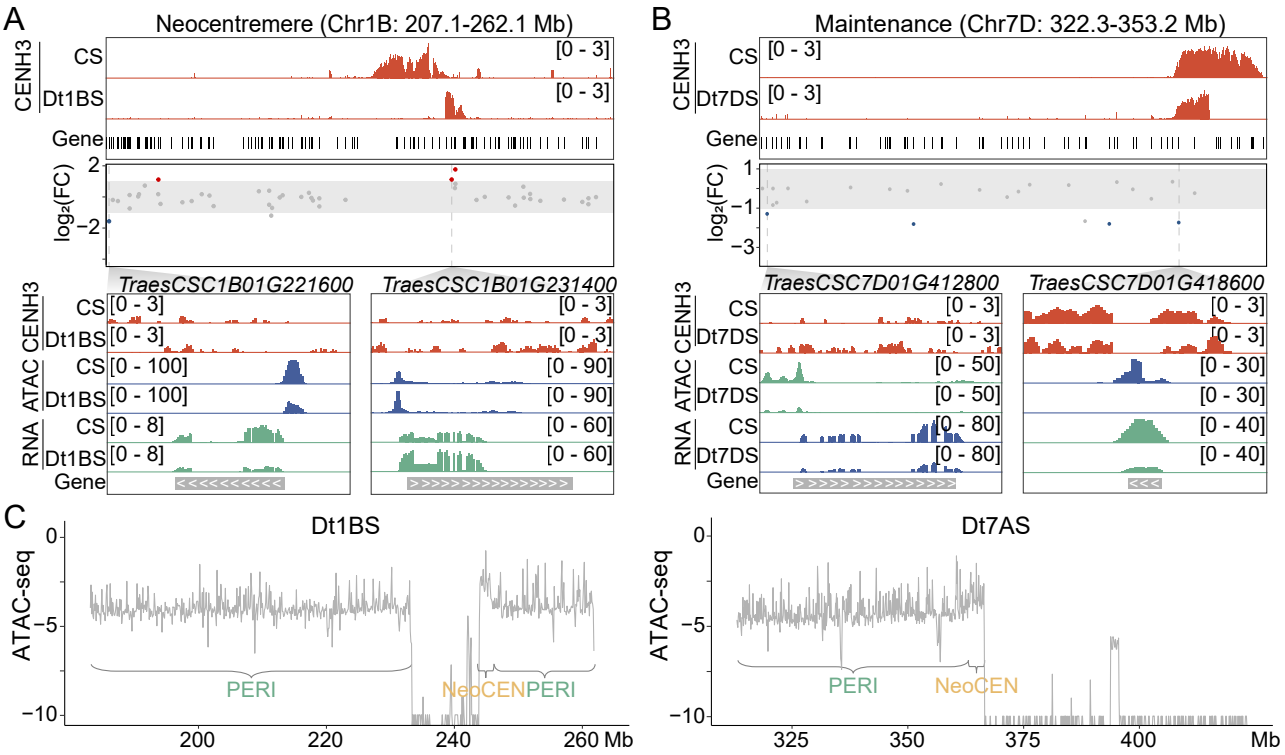

Supplemental Fig. S14. Coordinated gene expression and chromatin accessibility changes within (peri)centromeric regions in wheat ditelocentric lines. (A-B) Integrated Genome Viewer (IGV) snapshots show RNA-seq and ATAC-seq signals mapped to centromeric and pericentromeric regions in ditelosomic lines Dt1BS (A) and Dt7DS (B), in comparison to CS wheat. CENH3 ChIP-seq, ATAC-seq and RNA-seq data are displayed for each line. Genes with significant expression changes are color-coded: red dots for upregulated and blue dots for downregulated genes. Four representative genes — *TraesCSC1B01G221600*, *TraesCSC1B01G231400*, *TraesCSC7D01G412800* and *TraesCSC7D01G418600* — are highlighted with enlarged regional views to illustrate transcriptional and chromatin changes. The CENH3 profiles show clear centromere repositioning in ditelosomic chromosomes relative to CS. (C) Genome-wide normalized ATAC-seq signals comparisons across three chromatin domains — native centromere (CEN), neocentromere (NeoCEN), and pericentromeric heterochromatin (PERI) — in Dt1BS and Dt7AS lines. Data were averaged in 100-kb bins. Chromatin accessibility is elevated in neocentromeric regions compared to their flanking heterochromatic domains, suggesting that chromatin remodeling accompanies neocentromere formation. These results provide evidence of localized and coordinated changes in both gene expression and chromatin openness following centromere misdivision and reorganization.